Activities in $MnO-SiO_2-Al_2O_3$ Slags and Deoxidation Equilibria of Mn and Si

HIROKI OHTA and HIDEAKI SUITO

The activities of MnO and SiO_2 along the liquidus line in the $MnO-SiO_2-Al_2O_3-Fe_tO$ (1.2 to 6.7 mass pct) system were determined at 1823 and 1873 K by using a slag-metal equilibration technique. On the basis of the re-evaluated MnO iso-activity curves, the SiO_2 and Al_2O_3 iso-activity curves were determined by using the ternary Gibbs–Duhem relation. The control of inclusions composition in Si-Mn killed steels is discussed based on the equilibria between inclusion and steel with respect to Si, Mn, Al, and O.

I. INTRODUCTION

In the production of high-quality steels, the knowledge of the equilibrium between inclusions and steel is indispensable for the precise control of the composition of inclusions. In particular, the activities in the $MnO-SiO_2-Al_2O_3$ system are of essential importance in Mn-Si killed steels. Sharma and Richardson[1] measured the activities of MnO in this system with high MnO content at 1923 K by using a gas-slag-Pt equilibration technique. Fujisawa and Sakao[2] measured the activities of MnO and SiO_2 in this system at 1823 K along the liquidus line saturated with alumina. By using the ternary Gibbs–Duhem relation, they[3] evaluated the activities of MnO, SiO_2, and Al_2O_3 in the liquid region at 1823 and 1923 K, based on the MnO iso-activity curves obtained by Sharma and Richardson. However, there are no reported activity values in this system in the SiO_2-rich region, which are required for a clear understanding and the precise control of the inclusions composition.

In the present study, the activities of MnO and SiO_2 along the liquidus line in the $MnO-SiO_2-Al_2O_3-Fe_tO$ (1.2 to 6.7 mass pct) system, which is saturated with mullite and alumina, were determined at 1823 and 1873 K by using a slag-metal equilibration technique. On the basis of the activities of MnO reported by Sharma and Richardson[1] coupled with the present results, the MnO iso-activity curves were re-evaluated. Then, the activities of SiO_2 and Al_2O_3 were estimated from the MnO iso-activity curves by using the ternary Gibbs–Duhem relation, coupled with the present activities of SiO_2 along the liquidus line. Furthermore, the control of inclusions composition in Si-Mn killed steels is discussed based on the equilibrium between inclusion and steel with respect to Si, Mn, Al, and O.

II. EXPERIMENTAL

A. *Procedure*

The master slags were prepared by premelting the mixture of reagent grade Mn_2O_3, SiO_2, and Al_2O_3 in a Pt crucible under air. High-purity electrolytic iron (30 g) starting with approximately 500 to 1000 mass ppm oxygen and $MnO-SiO_2-Al_2O_3$ slag (7 g) was melted in an Al_2O_3 crucible at 1823 and 1873 K under deoxidized Ar atmosphere. An appropriate amount of Fe-1 mass pct Al, Fe-76 mass pct Si, and Fe-10 to 20 mass pct Mn alloys was added by dropping afterward. Then, the melts were stirred over a period of 2 to 5 hours by an Al_2O_3 rod for 90 seconds at 30-minute intervals. In previous slag-metal equilibrium experiments using $CaO-Al_2O_3$,[4] $CaO-Al_2O_3-MgO$,[5] and $CaO-Al_2O_3-SiO_2$ slags,[6] the time for attainment of equilibrium was confirmed to be within 1 hour. In the present work, the equilibrium time was chosen as 2 hours for the Al_2O_3-saturated slags and as 4 hours for the mullite-saturated slags with high viscosity. To eliminate oxide inclusions by flotation, the melts were unstirred for at least 1 hour before quenching. After equilibration, the crucible was taken out of the furnace and quenched rapidly in a He gas stream, followed by a water quenching.

B. *Chemical Analysis*

A detailed description of the chemical analyses for acid-soluble and acid-insoluble Mn,[7] Si,[8] Al,[9] and total oxygen[10] in metal phase and those for Mn,[7] Si,[8] Al,[9] and total Fe[11] in slag phase were already given in previous articles.

III. RESULTS AND DISCUSSION

The chemical compositions of slag and metal phases obtained in this work are summarized in Table I. The present slag compositions are plotted in the $MnO-SiO_2-Al_2O_3$ ternary diagram, as shown in Figure 1, although the present slags contain 1.2 to 6.7 mass pct Fe_tO. The liquidus compositions saturated with a mullite phase agree well with those reported by Muan and Osborn,[12] whereas those saturated with an alumina phase have a higher Al_2O_3 content in comparison with those by Muan and Osborn. The experimental slag compositions saturated with alumina by Fujisawa and Sakao[2] are indicated in Figure 1 by a shaded area. The liquidus compositions saturated with silica reported by Muan and Osborn[12] were used in the present study.

HIROKI OHTA, Research Associate, and HIDEAKI SUITO, Professor, are with the Institute for Advanced Materials Processing, Tohoku University, Sendai 980, Japan.

Manuscript submitted May 23, 1995.

Table I. Chemical Compositions of Metal and Slag Phases

Time (h)	Metal [Mn] (Mass Pct)	Metal [Si] (Mass Pct)	Metal [Al] Soluble (Mass Ppm)	Metal [Al] Insoluble (Mass Ppm)	Metal [O] (Mass Ppm)	Slag (MnO)	Slag (SiO_2) (Mass Pct)	Slag (Al_2O_3) (Mass Pct)	Slag (Fe_tO) (Mass Pct)
1823 K									
Slag a-1									
5	0.184	0.527	2.6	0.9	34.8	14.9	53.6	26.3	3.79
5	0.272	1.13	6.6	1.4	26.6	14.9	54.8	26.4	2.34
5	0.315	1.42	7.5	2.1	26.0	14.9	54.8	26.9	2.04
Slag b-1									
4	0.215	0.327	3.4	0.7	38.4	18.8	42.3	34.1	4.13
4	0.297	0.521	0.9	3.6	31.9	20.8	43.2	34.0	3.20
4	0.463	1.18	3.4	5.9	23.5	20.9	44.7	32.6	1.95
4	0.484	1.27	6.1	5.3	23.0	20.6	43.0	32.3	1.72
Slag c-1									
4	0.192	0.176	2.8	0.3	49.2	20.0	39.7	36.2	4.69
4	0.237	0.254	1.5	1.4	39.9	20.9	38.5	36.4	4.10
4	0.470	0.911	5.4	1.7	24.3	21.3	41.0	35.1	1.96
4	0.593	1.31	6.1	2.5	22.2	21.4	40.7	35.6	1.60
Slag d-1									
3	0.317	0.092	0.4	1.7	54.8	25.2	30.3	40.4	4.70
2	0.517	0.252	1.9	1.8	34.8	25.0	31.3	39.8	2.71
2	0.500	0.221	2.5	1.6	35.8	24.6	31.2	39.5	3.04
2	1.13	1.06	5.8	3.8	20.5	25.1	31.9	40.2	1.18
1873 K									
Slag a-2									
4	0.173	0.578	3.8	2.4	53.7	14.2	50.4	31.2	4.20
4	0.179	0.607	4.0	3.3	53.3	14.3	51.2	29.7	4.11
4.5	0.306	1.39	8.9	3.0	38.9	15.0	52.2	29.3	2.57
Slag b-2									
4.5	0.135	0.165	4.6	0.3	79.3	18.1	41.7	35.7	4.69
4.5	0.177	0.366	4.3	1.2	60.6	18.1	42.7	35.6	3.79
4.5	0.257	0.724	7.8	0.3	46.9	17.7	44.4	34.4	3.02
Slag c-2									
5	0.236	0.433	2.4	4.7	53.2	18.7	38.4	39.3	4.39
4	0.276	0.526	2.1	4.8	48.7	18.9	38.5	40.2	3.63
4	0.424	1.18	6.4	7.2	37.3	18.8	38.6	40.4	2.19
4.5	0.481	1.45	7.7	5.9	35.8	20.0	40.5	38.5	2.30
Slag d-2									
3	0.192	0.185	1.3	2.2	73.8	18.9	34.5	40.3	5.91
3	0.192	0.189	2.9	1.0	74.3	19.3	34.8	39.9	5.72
3	0.263	0.370	3.5	3.5	52.4	20.0	35.6	40.4	4.12
3	0.403	0.766	7.4	4.1	39.4	19.6	36.6	40.6	2.64
Slag e-2									
3	0.253	0.062	1.7	0.5	101	23.2	27.5	42.1	6.72
3	0.280	0.076	1.4	1.1	95.9	25.2	30.0	44.5	*
3	0.467	0.195	3.4	1.5	62.4	24.3	29.5	43.4	3.68
3	0.420	0.161	2.6	1.2	68.2	23.8	28.9	42.4	4.31
Slag f-2									
2	0.763	0.034	3.9	0.2	101	30.5	16.8	47.8	5.27
2	1.34	0.113	7.8	0.2	55.1	30.9	16.4	48.5	4.09
2	0.509	0.015	3.0	0.3	144	30.7	16.9	48.6	4.37

*Not analyzed.

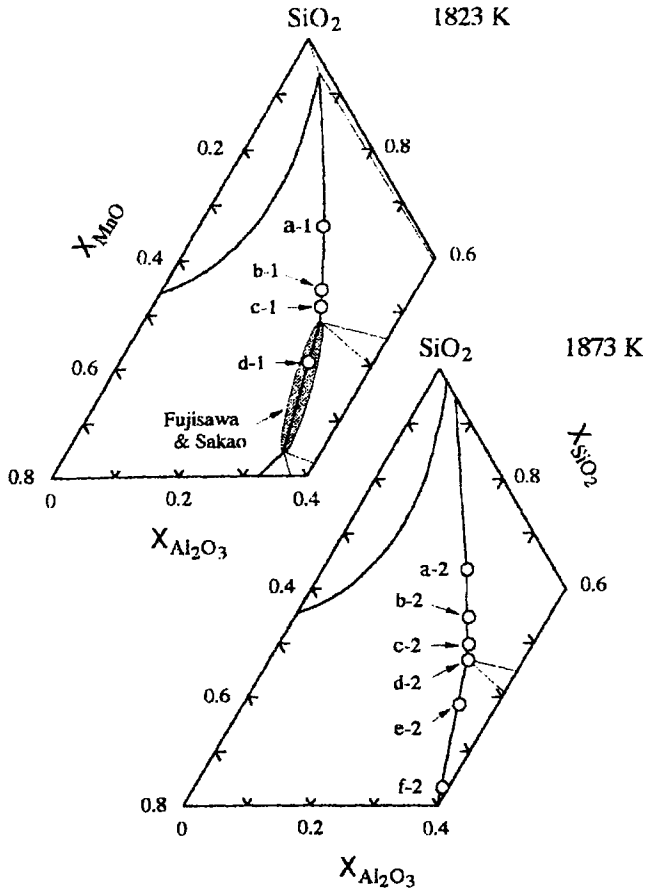

Fig. 1—Slag compositions used in the present work.

Table II. Interaction Parameters Used in the Present Work[14]

i	*j*	e_i^j	(r_i^j)
Al	Al	$0.011 + 63/T$	$(-0.0011 + 0.17/T)$
	Si	0.056	(−0.0006)
	O	$11.95 - 34{,}740/T$	
	C	0.091	(−0.004)
Si	Al	0.058	
	Si	$0.089 + 34.5/T$	$(-0.0055 + 6.5/T)$
	O	−0.23	
	Mn	0.002	
	C	$-0.023 + 380/T$	
O	Al	$7.15 - 20{,}600/T$	(1.7)
	Si	−0.131	
	O	$0.734 - 1750/T$	
	Mn	−0.021	
	C	−0.436*	
Mn	Si	0	
	O	−0.083	
	Mn	0	
	C	−0.07	

*Reference 15.

A. *Activities of SiO_2 and MnO along the Liquidus Line*

Silicon deoxidation equilibrium can be written as

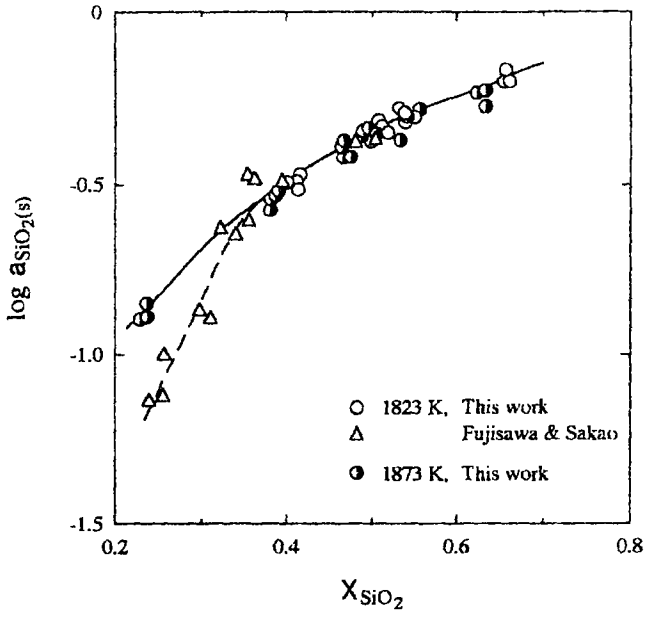

Fig. 2—Activities of SiO_2 in logarithmic form on the liquidus line saturated with mullite and alumina.

$$\underline{Si} + 2\underline{O} = SiO_2\ (s) \qquad [1]$$

$$\Delta G^\circ_1 = -581{,}900 + 221.8T \quad \text{J/mol}^{[13,14]}$$

The activities of SiO_2, a_{SiO_2}, relative to the solid standard state were calculated from the ΔG°_1 value, the metal compositions given in Table I, and the respective interaction coefficients for $f_{\underline{Si}}$ and $f_{\underline{O}}$ with respect to a dilute solution of 1 mass pct standard state, which are given in Table II. In the case of the interaction coefficients whose temperature dependencies were not reported, the values at 1823 K were estimated from those at 1873 K given in Table II by assuming a regular solution. The calculated values of a_{SiO_2} in logarithmic form are plotted against the mole fraction of SiO_2, X_{SiO_2}, in the $MnO\text{-}SiO_2\text{-}Al_2O_3$ ternary system, as shown in Figure 2. It can be seen that no temperature dependence of a_{SiO_2} was observed in the range of $X_{SiO_2} \geq 0.4$ saturated with mullite, but in the range below this value, the present values at 1873 K are higher than those obtained by Fujisawa and Sakao.[2]

Manganese deoxidation equilibrium can be expressed by

$$\underline{Mn} + \underline{O} = MnO\ (s) \qquad [2]$$

$$\Delta G^\circ_2 = -288{,}100 + 128.3T \quad \text{J/mol}^{[16]}$$

The a_{MnO} values relative to the solid standard state were obtained from the ΔG°_2 value, the compositions of metal phase, and the respective interaction coefficients for $f_{\underline{Mn}}$ and $f_{\underline{O}}$. These results are shown in Figure 3, in which the temperature dependence of a_{MnO} is clearly demonstrated and the slope in the plot of log a_{MnO} *vs* X_{SiO_2} changes at the composition double saturated with mullite and alumina phases, as indicated by an arrow.

From Eqs. [1] and [2], one obtains

$$MnO\ (s) + 1/2\ \underline{Si} = \underline{Mn} + 1/2\ SiO_2\ (s) \qquad [3]$$

The following relation can be deduced from Eq. [3], using the equilibrium constant, K_3, for Reaction [3].

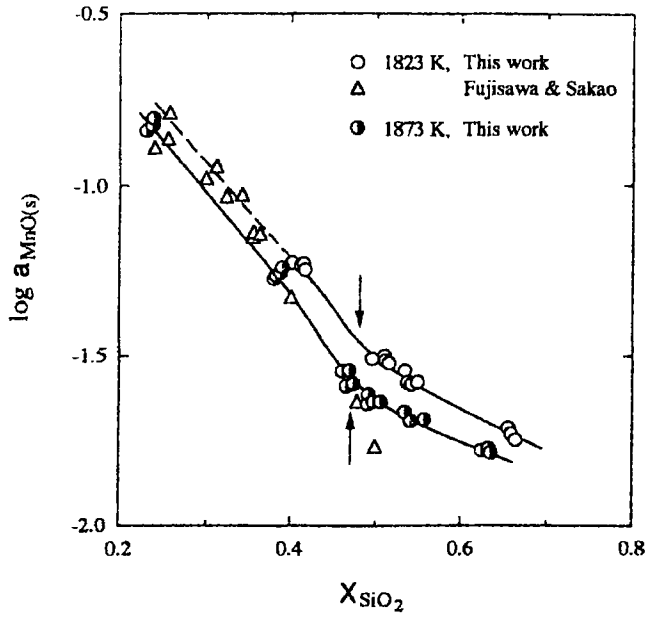

Fig. 3—Activities of MnO in logarithmic form on the liquidus line saturated with mullite and alumina.

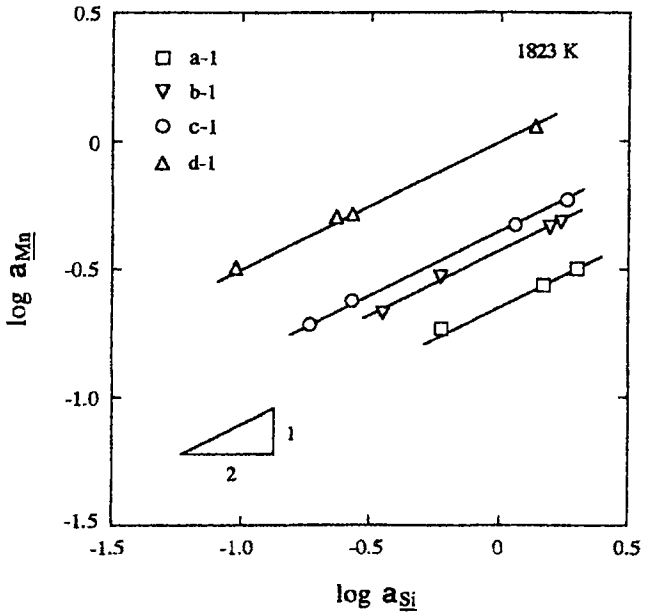

Fig. 4—Relation between activities of Mn and Si in logarithmic form at 1823 K. The marks a-1 through d-1 denote the slag compositions indicated in Fig. 1.

$$\log a_{\underline{Mn}} = (1/2) \log a_{\underline{Si}} - \log \{a_{SiO_2}^{1/2} / (a_{MnO} \cdot K_3)\} \quad [4]$$

The activities of Mn and Si at 1823 K were estimated at a given slag composition (a-1 through d-1 in Figure 1) by using the respective interaction coefficients given in Table II. These values in logarithmic form are shown in Figure 4, indicating a linear relationship with a slope of 1/2, as predicted from Eq. [4]. The linear relations were also observed for the slags of a-2 through f-2 indicated in Figure 1.

B. *Activities of Al_2O_3 along the Liquidus Line*

The $a_{Al_2O_3}$ values relative to the solid standard state can be estimated from the ΔG°_{Al} (= −1,202,000 + 386.3 T J/mol[13,14]) value for the reaction $2\underline{Al} + 3\underline{O} = Al_2O_3$ (s), using the compositions of metal phase and the respective interaction coefficients. It was found, however, that the $a_{Al_2O_3}$ values in the mullite-saturated slags could not be accurately determined because of considerably low contents of Al (3 to 12 mass ppm), as given in Table I. For this reason, the $a_{Al_2O_3}$ values were estimated from the $\Delta G^\circ_{mullite}$ (= −4,350 + 10.5 T J/mol[17]) value for the formation of mullite, $3Al_2O_3 \cdot 2SiO_2$, by using the present values of a_{SiO_2}. However, since the previously mentioned value for $\Delta G^\circ_{mullite}$ was obtained at the slag composition saturated with alumina, the $a_{Al_2O_3}$ values on the liquidus line saturated with mullite should not be derived from the $\Delta G^\circ_{mullite}$ value by using the experimentally determined values for a_{SiO_2}.

The a_{SiO_2} value at the d-2 slag composition double saturated with alumina and mullite was calculated from the $\Delta G^\circ_{mullite}$ value and $a_{Al_2O_3} = 1$. This value (log a_{SiO_2} = −0.335) was found to be in reasonable agreement with that (log a_{SiO_2} = −0.357 ± 0.07) calculated from Eq. [1].

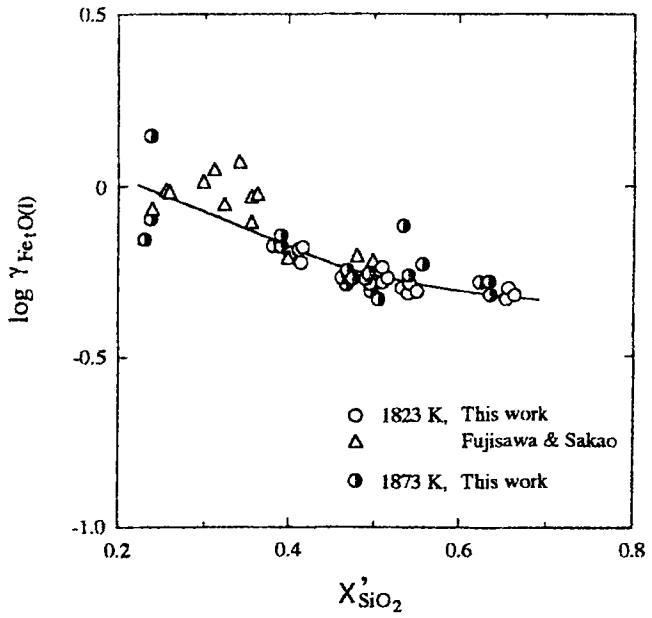

Fig. 5—Activity coefficient of Fe_tO in logarithmic form on the liquidus line saturated with mullite and alumina.

C. *Activity Coefficient of Fe_tO along the Liquidus Line*

The activity coefficients of Fe_tO, γ_{Fe_tO}, relative to the liquid standard state were calculated from Eq. [5] by using the compositions of metal phase, the content of Fe_tO, and the interaction coefficients for $f_{\underline{O}}$.

$$Fe\ (l) + \underline{O} = Fe_tO\ (l) \quad [5]$$

$$\Delta G^\circ_5 = -116{,}100 + 48.79T \quad J/mol[18]$$

The calculated results for log γ_{Fe_tO} are plotted against the mole fraction of SiO_2, X'_{SiO_2}, in the $MnO\text{-}SiO_2\text{-}Al_2O_3\text{-}Fe_tO$ quaternary system in Figure 5. It can be seen that the activity coefficients of Fe_tO decrease with an increase in the SiO_2 content along the liquidus line, and no temperature dependence of activity coefficients was observed, although the data scatter to a significant degree.

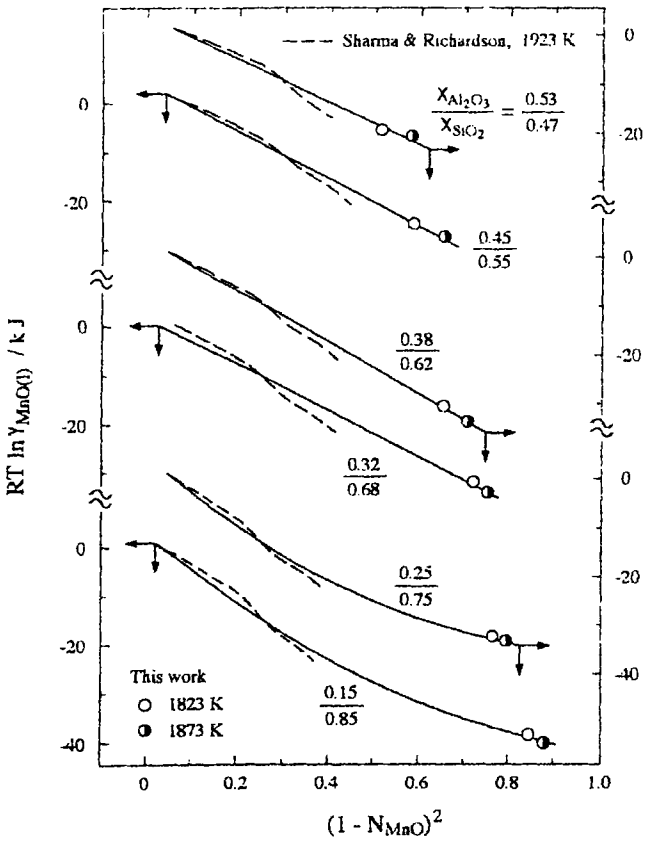

Fig. 6—Plots for the relation given by Eq. [7].

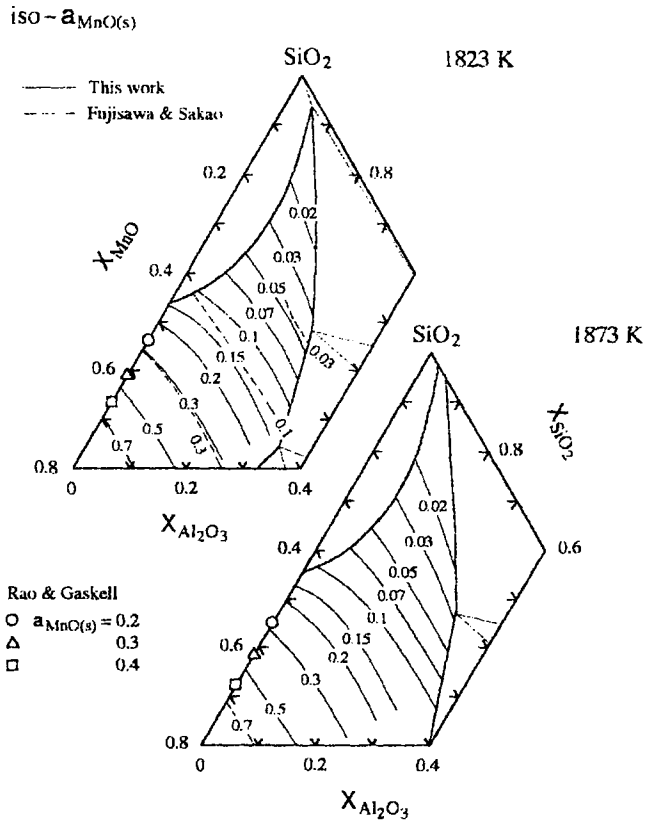

Fig. 7—MnO iso-activity curves at 1823 and 1873 K. The broken lines represent the values of a_{MnO} obtained by Fujisawa and Sakao.[3]

D. *Estimation of Activities by the Gibbs–Duhem Relation*

Sharma and Richardson[1] measured the activities of MnO in the MnO-SiO_2-Al_2O_3 slags with the compositions of $X_{SiO_2} \leq 0.5$ and $X_{MnO} \leq 0.8$ by using a gas-slag-Pt equilibration technique at 1923 K. In order to estimate the a_{MnO} values in the SiO_2-rich region at a given temperature, the applicability of the ternary regular solution model to the present slag system was studied by using the present and Sharma and Richardson's[1] data in the following discussion.

The activity coefficient of MnO relative to the liquid standard state in the ternary regular solution can be represented by

$$RT \ln \gamma_{MnO(l)} = \alpha N_{SiO_2}^2 + \beta N_{AlO_{1.5}}^2 + \delta N_{SiO_2} \cdot N_{AlO_{1.5}} + I \quad [6]$$

where α, β, and δ are constants relating to the interaction parameters in the binary regular solution, I is a constant, and N is the mole fraction in the MnO-SiO_2-$AlO_{1.5}$ ternary system.

Equation [6] can be deduced under the constant $N_{AlO_{1.5}}/N_{SiO_2}$ ratio as follows:

$$RT \ln \gamma_{MnO(l)} = a (1 - N_{MnO})^2 + b \quad [7]$$

where a and b are constants.

The present and previous results[1] for a_{MnO}, which were obtained relative to the solid standard state, were converted to those relative to the liquid standard state by using the free energy change of fusion: MnO (s) = MnO (l); ΔG° = 43,930 − 20.77 T J/mol.[19] The validity of the relation given by Eq. [7] was examined as a function of the $X_{Al_2O_3}/X_{SiO_2}$ ratio in Figure 6. It can be seen that the present results do not fall on the line obtained by linearly extrapolating the data by Sharma and Richardson[1] in the range of $X_{Al_2O_3}/X_{SiO_2} \leq 0.25/0.75$, while in the range above this ratio, the present results fall approximately on the linearly extrapolated line. The values of a_{MnO} estimated from the lines in Figure 6 agree with those of Sharma and Richardson within the maximum limit of error of log $a_{MnO(s)} = \pm 0.11$.

The results in Figure 6 indicate that the regular solution model can be applied with respect to the activity of MnO in only a limited range of slag compositions. Therefore, the activities of MnO in the MnO-SiO_2-Al_2O_3 ternary system were determined not from a regular solution parameter but from the lines in the plot of RT ln $\gamma_{MnO(l)}$ *vs* $(1 - N_{MnO})^2$ for various $X_{Al_2O_3}/X_{SiO_2}$ ratios. The linear and quadratic regression analyses were used for the data in the ranges of $X_{Al_2O_3}/X_{SiO_2} \geq 0.32/0.68$ and $\leq 0.25/0.75$, respectively. The iso-a_{MnO} curves at 1823 and 1873 K are obtained, as shown in Figure 7, in which the results[20] in the MnO-SiO_2 system are also indicated by open marks. Fujisawa and Sakao[3] calculated the a_{MnO} values at slag compositions of $N_{SiO_2} \leq 0.6$, on the basis of the data of Sharma and Richardson,[1] by assuming a regular solution. Their calculated values for $a_{MnO(s)}$ (=0.03, 0.1, and 0.3) at 1823 K are also indicated by broken lines in Figure 7.

The activities of SiO_2 were estimated from the iso-a_{MnO} curves by using the Schuhmann method[21] given by Eq. [8]:

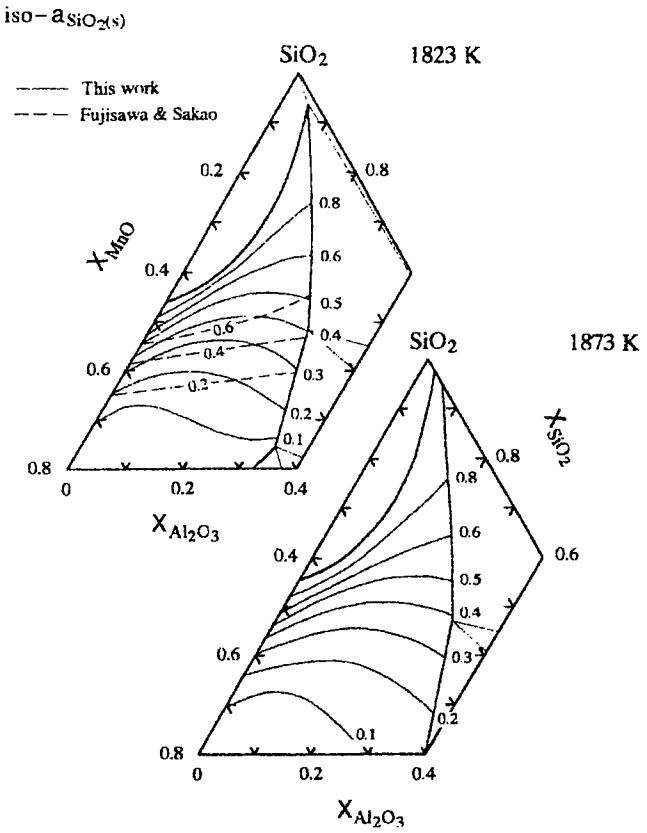

Fig. 8—SiO_2 iso-activity curves at 1823 and 1873 K. The broken lines represent the values of a_{SiO_2} obtained by Fujisawa and Sakao.[3]

$$\log a^{II}_{SiO_2} = \log a^{I}_{SiO_2} - \int_{\log a^{I}_{MnO}}^{\log a^{II}_{MnO}} \left(\frac{\delta n_{MnO}}{\delta n_{SiO_2}}\right)_{a_{MnO},\, n_{Al_2O_3}} d \log a_{MnO} \quad [8]$$

where $a^{I}_{SiO_2}$ and $a^{II}_{SiO_2}$ are the activities of SiO_2 at initial and final states, respectively, that is, the integration limit, and n_i is the number of moles of component i.

In the present calculation, the a_{SiO_2} values on the SiO_2-saturated liquidus line reported by Muan and Osborn[12] and those on the liquidus lines saturated with mullite and alumina determined in this work were used for the $a^{I}_{SiO_2}$ values. The resulting iso-a_{SiO_2} curves are shown in Figure 8, together with the results obtained by Fujisawa and Sakao[3] (a_{SiO_2} = 0.2, 0.4, and 0.6) indicated by broken lines. It can be seen that the γ_{SiO_2} values tend to decrease with an increase in the SiO_2 content, as compared with the results by Fujisawa and Sakao.

The iso-$a_{Al_2O_3}$ curves were determined as follows. In the case that the $a_{Al_2O_3}$ values are determined from the iso-a_{MnO} curves in a manner similar to the estimation of a_{SiO_2} values, the available integration limit at the initial stage ($a^{I}_{Al_2O_3}$) is limited to only the liquidus lines saturated with alumina. This leads to the evaluation of the iso-$a_{Al_2O_3}$ curves in the limited region of slag composition. Therefore, the $a_{Al_2O_3}$ values on the line joining a certain slag composition saturated with Al_2O_3 with the SiO_2 apex in the ternary diagram were first estimated by the Schuhmann method[21] using the iso-a_{SiO_2} curves, as shown schematically in Figure 9. These values for $a_{Al_2O_3}$ along with those on the Al_2O_3-saturated line were used as the integration limit at the initial stage and

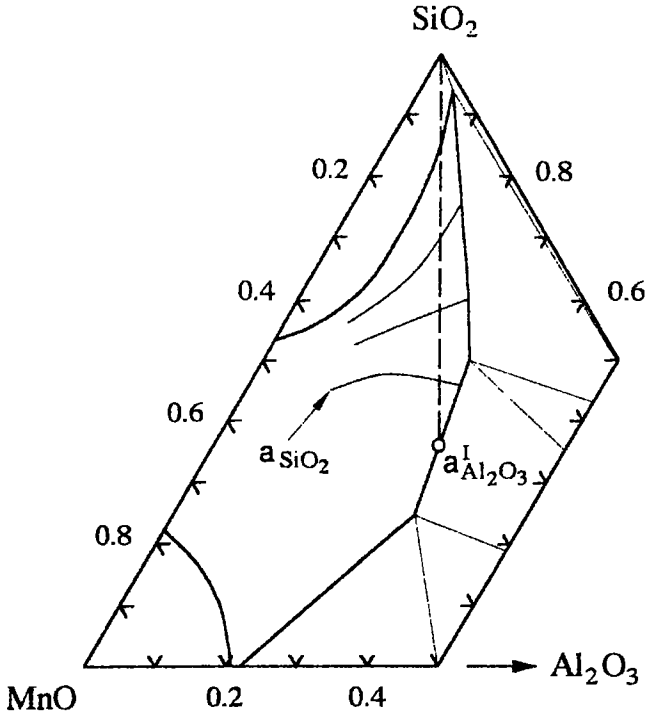

Fig. 9—Schematic representation for obtaining the integration lower limit of $a^{I}_{Al_2O_3}$ by using the iso-a_{SiO_2} curves.

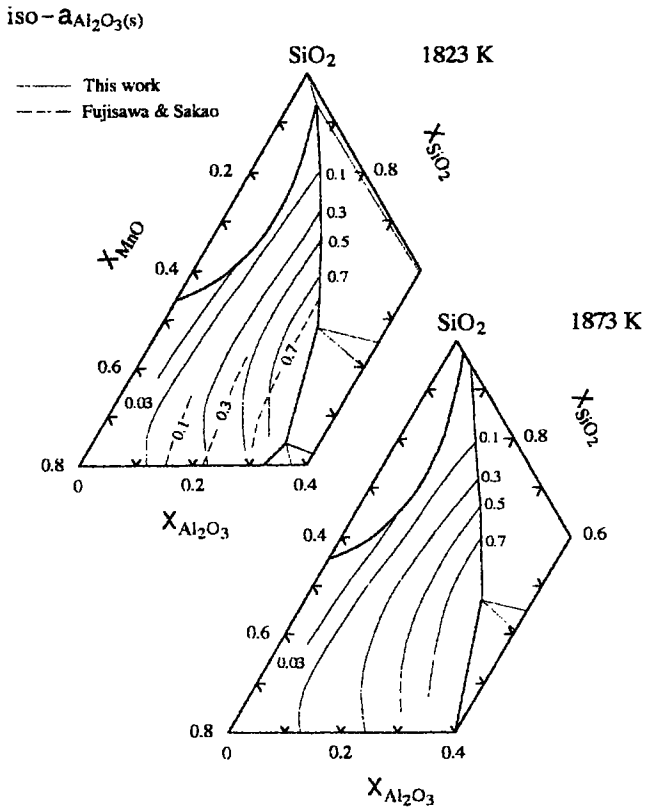

Fig. 10—Al_2O_3 iso-activity curves at 1823 and 1873 K. The broken lines represent the values of $a_{Al_2O_3}$ obtained by Fujisawa and Sakao.[3]

then the calculations of the iso-$a_{Al_2O_3}$ curves were made based on the iso-a_{MnO} curves. The maximum limit of errors in the $a_{Al_2O_3}$ values obtained by the present method arises

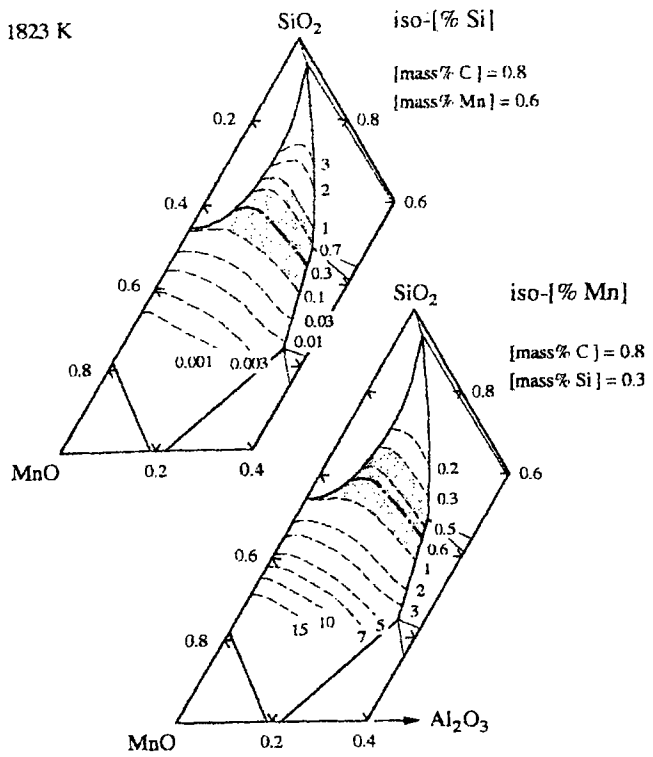

Fig. 11—Iso-Mn content curves at [mass pct Si] = 0.3 and [mass pct C] = 0.8, and iso-Si content curves at [mass pct Mn] = 0.6 and [mass pct C] = 0.8. The heavy dash-dotted lines correspond to the compositions calculated at [mass pct Si] = 0.3, [mass pct Mn] = 0.6, and [mass pct C] = 0.8.

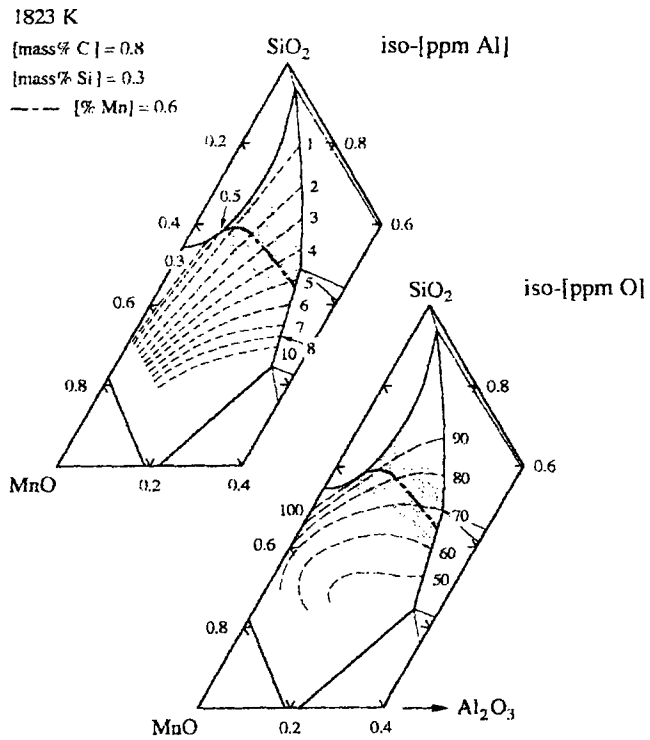

Fig. 12—Iso-Al and iso-O content curves at [mass pct Si] = 0.3 and [mass pct C] = 0.8.

from those in the values of a_{MnO} and a_{SiO_2}. The maximum limit of errors in a_{MnO} values was estimated as log a_{MnO} = ± 0.11, as mentioned previously. The maximum limit of errors in a_{SiO_2} values is mostly due to the experimental uncertainty which is estimated as log $a_{SiO_2} = \pm 0.02$. Consequently, the maximum limit of errors in $a_{Al_2O_3}$ values is calculated as log $a_{Al_2O_3} = \pm 0.13$. The results are shown in Figure 10, in which the values by Fujisawa and Sakao[3] ($a_{Al_2O_3}$ = 0.1, 0.3, and 0.7 at 1823 K) are also indicated by broken lines. Fujisawa and Sakao report the $a_{Al_2O_3}$ values in the limited range of slag composition, and their values are found to be slightly greater than the present results. However, the difference between the two is within the limit of the estimated errors in $a_{Al_2O_3}$ values.

E. *Deoxidation Equilibria of Si and Mn*

The equilibrium between inclusions and high carbon Mn-Si killed steels was studied with the focus on the influence of the contents of Al and O on the inclusions composition. In the following calculations, the steel containing Si = 0.3, Mn = 0.6, and C = 0.8 in mass pct was chosen as one of the Mn-Si killed steels.

The contents of Al, Mn, and O in equilibrium with a given inclusion composition were calculated at 1823 K by the following iterative method at the constant contents of [mass pct C] = 0.8 and [mass pct Si] = 0.3. The Al contents at a given composition were first estimated from the reaction $\underline{Al} + 3/4SiO_2$ (s) = $3/4\underline{Si} + 1/2Al_2O_3$ (s), $\Delta G^\circ = -164{,}600 + 26.8\ T$ J/mol[13,14] by using the values for $a_{Al_2O_3}$ and a_{SiO_2} and the respective interaction coefficients for $f_{\underline{Si}}$ and $f_{\underline{Al}}$ given in Table II. Then, the Mn contents were calculated from Reaction [3] by taking into account the previously mentioned Al contents, coupled with the respective interaction coefficients for $f_{\underline{Mn}}$ and $f_{\underline{Si}}$. Finally, the O contents were determined from Reaction [1] by using [mass pct Si] = 0.3 and the previously mentioned values for the Al and Mn contents. This procedure for the calculation was repeated until the values for Al, Mn, and O contents became constant. These values at the constant contents of [mass pct C] = 0.8 and [mass pct Si] = 0.3 were determined as a function of inclusion composition, and the iso-Mn content curves are shown in the lower diagram in Figure 11.

The upper diagram in Figure 11 shows the iso-Si content curves at the constant contents of [mass pct C] = 0.8 and [mass pct Mn] = 0.6 at 1823 K in a manner similar to the previously mentioned iterative method. It follows from the results in Figure 11 that the inclusion composition becomes rich in the SiO_2 content with a decrease in the Mn content at constant contents of [mass pct C] = 0.8 and [mass pct Si] = 0.3, while at constant contents of [mass pct C] = 0.8 and [mass pct Mn] = 0.6, the inclusion compositions also become rich in the SiO_2 content with an increase in the Si content. The heavy dash-dotted lines correspond to the inclusion compositions in equilibrium with the steel of [mass pct C] = 0.8, [mass pct Mn] = 0.6, and [mass pct Si] = 0.3. The shaded area in the lower diagram in Figure 11 corresponds to the inclusion compositions in equilibrium with the steel of [mass pct Mn] = 0.3 to 1, [mass pct Si] = 0.3, and [mass pct C] = 0.8. The shaded area in the upper diagram in Figure 11 corresponds to the inclusion compositions in equilibrium with the steel of [mass pct Si] = 0.1 to 1, [mass pct Mn] = 0.6, and [mass pct C] = 0.8.

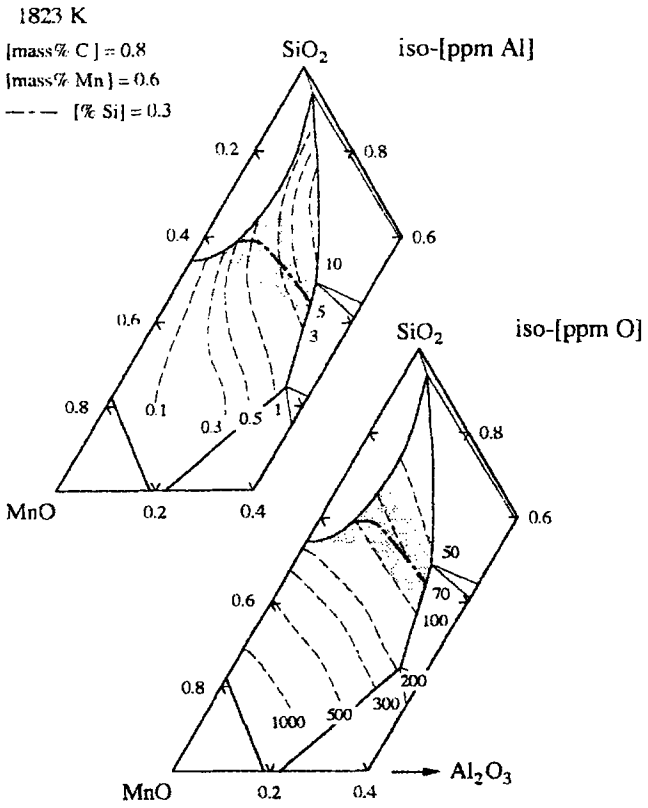

Fig. 13—Iso-Al and iso-O content curves at [mass pct Mn] = 0.6 and [mass pct C] = 0.8.

It can be concluded that the inclusion composition lies within the shaded area in Figure 11, when the contents of Si and Mn in high carbon steels are in the range between 0.1 (0.3) and 1 mass pct, respectively.

The iso-Al and iso-O content curves at the constant contents of [mass pct Si] = 0.3 and [mass pct C] = 0.8 are shown in the upper and lower diagrams in Figure 12, respectively. The heavy dash-dotted lines and the shaded areas have the same meanings as in Figure 11. It can be seen that the Al or O level must be fixed in order to have a certain composition of inclusion on the heavy dash-dotted line. Furthermore, when the inclusion composition moves along the heavy dash-dotted line from left to right, the Al and O contents change from 0.5 to 5 and 100 to 65 mass ppm, respectively.

The iso-Al and iso-O content curves at the constant contents of [mass pct Mn] = 0.6 and [mass pct C] = 0.8 are shown in the upper and lower diagrams in Figure 13, respectively. The heavy dash-dotted lines and the shaded areas have the same meanings as in Figure 11. It should be noted that the iso-Al and iso-O content curves indicate different behaviors from those in Figure 12, and the Al and O contents within the shaded areas are below 10 and 50 to 190 mass ppm, respectively.

In order to have "soft" inclusion dispersions, that is, the deformable inclusions during hot rolling in high carbon Si-Mn killed steel, the Al level must be controlled within a narrow range, such as the shaded areas in Figures 11 and 12, although the oxygen level is considerably high.

IV. CONCLUSIONS

Based on the results of Sharma and Richardson[1] at 1923 K, coupled with the present results obtained by a slag-metal equilibration technique at 1823 and 1873 K, the activities of MnO in the $MnO-SiO_2-Al_2O_3$ system were determined from the relations between $RT \ln \gamma_{MnO(l)}$ and $(1 - N_{MnO})^2$. The present results for a_{MnO} are found to be in close agreement with those of Fujisawa and Sakao[2] at the slag compositions below $N_{SiO_2} = 0.5$, but in the range above $N_{SiO_2} = 0.5$, the present a_{MnO} values are different from their values obtained by extrapolating the values of Sharma and Richardson. The values of a_{SiO_2} and $a_{Al_2O_3}$ determined by the Schuhmann method are in reasonable agreement with the values obtained by Fujisawa and Sakao. The thermochemical data on the compounds and experimentation of the liquidus line saturated with SiO_2 in the $MnO-SiO_2-Al_2O_3$ system are required for the improvement in accuracy of the activity values.

REFERENCES

1. R.A. Sharma and F.D. Richardson: *Trans. TMS-AIME*, 1965, vol. 233, pp. 1586-92.
2. T. Fujisawa and H. Sakao: *Tetsu-to-Hagané*, 1977, vol. 63, pp. 1504-11.
3. T. Fujisawa and H. Sakao: *Tetsu-to-Hagané*, 1977, vol. 63, pp. 1493-1503.
4. T. Kimura and H. Suito: *Metall. Mater. Trans. B*, 1994, vol. 25B, pp. 33-42.
5. R. Inoue and H. Suito: *Metall. Mater. Trans. B*, 1994, vol. 25B, pp. 235-44.
6. F. Tamura and H. Suito: *Metall. Mater. Trans. B*, 1993, vol. 24B, pp. 121-30.
7. H. Ohta and H. Suito: *Metall. Mater. Trans. B*, 1995, vol. 26B, pp. 295-303.
8. R. Inoue and H. Suito: *Metall. Trans. B*, 1992, vol. 23B, pp. 613-21.
9. H. Suito, H. Inoue, and R. Inoue: *Iron Steel Inst. Jpn. Int.*, 1991, vol. 31, pp. 1381-88.
10. R. Inoue and H. Suito: *Mater. Trans. Jpn. Inst. Met.*, 1991, vol. 32, pp. 1164-69.
11. K.R. Lee and H. Suito: *Metall. Mater. Trans. B*, 1994, vol. 25B, pp. 893-902.
12. A. Muan and E.F. Osborn: *Phase Equilibria among Oxides in Steelmaking*, Addison-Wesley Publishing Co., Reading, MA, 1965.
13. J.F. Elliott, M. Gleiser, and V. Ramakrishna: *Thermochemistry for Steelmaking*, Addison-Wesley Publishing Co., Reading, MA, 1963, vol. 2.
14. G.K. Sigworth and J.F. Elliott: *Met. Sci.*, 1974, vol. 8, pp. 298-310.
15. S. Ban-ya and S. Matoba: *Tetsu-to-Hagané*, 1962, vol. 48, pp. 925-32.
16. H. Gaye, C. Gatellier, M. Nadif, P.V. Riboud, J. Saleil, and M. Faral: *Rev. Metall. -CIT*, 1987, Nov., pp. 759-71.
17. R.H. Rein and J. Chipman: *Trans. TMS-AIME*, 1965, vol. 233, pp. 415-25.
18. H. Suito and R. Inoue: *Trans. Iron Steel Inst. Jpn.*, 1984, vol. 24, pp. 301-07.
19. I. Barin and O. Knack: *Thermochemical Properties of Inorganic Substances*, Springer-Verlag, New York, NY, 1973.
20. B.K.D.P. Rao and D.R. Gaskell: *Metall. Trans. B*, 1981, vol. 12B, pp. 311-17.
21. R. Schuhmann: *Acta. Met.*, 1955, vol. 3, pp. 219-26.